Steel and Composite Structures, *Vol. 29, No. 4 (2018) 437-450*
DOI: https://doi.org/10.12989/scs.2018.29.4.437

Parameters influencing redundancy of twin steel box-girder bridges

Janghwan Kim [1a], Seong-Hoon Kee [2b], Heejung Youn [3c] and Dae Young Kim [*4]

[1] *Dealim Industrial Corporation Ltd., Seoul 03152, Republic of Korea*
[2] *Department of Architectural Engineering, Dong-A University, Busan 121-791, Republic of Korea*
[3] *Department of Civil Engineering, Hongik University, Seoul 04066, Republic of Korea*
[4] *Department of Architectural Engineering, Pusan National University, Busan 130-743, Republic of Korea*

(*Received December 27, 2017, Revised September 29, 2018, Accepted November 8, 2018*)

Abstract. A bridge comprising of two girders, such as a twin steel box-girder bridge, is classified as fracture critical (i.e., non-redundant). In this study, the various bridge components of the twin steel box-girder bridge are investigated to determine if these could be utilized to improve bridge redundancy. Detailed finite-element (FE) models, capable of simulating prominent failure modes observed in a full-scale bridge fracture test, are utilized to evaluate the contributions of the bridge components on the ultimate behavior and redundancy of the bridge sustaining a fracture on one of its girders. The FE models incorporate material nonlinearities of the steel and concrete members, and are capable of capturing the effects of the stud connection failure and railing contact. Analysis results show that the increased tensile strength of the stud connection and (or) concrete strength are effective in improving bridge redundancy. By modulating these factors, redundancy could be significantly enhanced to the extent that the bridge may be excluded from its fracture critical designation.

Keywords: bridge safety; redundancy; ultimate capacity; bridge collapse; composite bridge

1. Introduction

Bridge redundancy can be referred to as the load-carrying capacity of a bridge without undergoing excessive deformations after suffering a failure of one or more main structural members. According to the AASHTO LRFD Bridge Design Specification (2014), two-girder bridges are classified as fracture critical (i.e., non-redundant), implying that the failure of the main members leads to bridge collapse. Bridge collapse does not only directly cause a large number of casualties, but also induces the indirect loss of road-user costs. For this reason, the AASHTO LRFD Specification (2014) requires more stringent fabrication and material provisions to increase bridge safety for a non-redundant bridge than for one that is redundant. Furthermore, this type of bridge requires more frequent and detailed inspections, such as biennial hands-on and nondestructive inspections on welded connections, which cost from two to five times the inspection cost of a redundant bridge (Connor *et al*. 2005). However, despite the non-redundant classification of two-girder bridges, several historical incidents involving the failure of the main members in steel plate girder bridges, such as the US 422 Bridge (Connor *et al*. 2007) and the I-794 Hoan Bridge (Hesse *et al*. 2014), have demonstrated that they could reserve significant load-carrying capacity. Compared with steel plate girder bridges, steel box-girder bridges have higher torsional stiffness and more structural elements that might contribute to load redistribution in the event of a fracture in one or more of its main members. Therefore, there is a high possibility that steel box-girder bridges with two girders may reserve a sufficient load-carrying capacity so as to be redundant. Accordingly, in view of the high maintenance costs associated with non-redundant bridges, it is worth accurately evaluating the redundancy of bridge systems and finding a method to improve it.

Ghosn and Moses (1998) initiated the attempt to quantitatively evaluate the redundancy of a two girder bridge. They proposed three system reserve factors as redundancy evaluation criteria using a probabilistic method based on the assumption that a four girder bridge is always redundant. These factors limit the ultimate strength and displacement for the two girder bridge to be redundant. Pham *et al*. (2014) evaluated the redundancy of two I-girder bridges based on these criteria. They found that the two I-girder bridges are not always redundant depending on the level of damage on the one of two girders.

For the redundancy evaluation of steel box-girder bridges, a simplified evaluation method was proposed by Samaras *et al*. (2012). They suggested that a twin steel box-girder bridge is redundant if it satisfies the strength checks on the intact girder, deck, and stud connections of the bridge. Based on this method, however, the displacement of the bridge could not be evaluated although it is one of important factors for public safety. Kim and Williamson (2015) suggested a deterministic method to evaluate the

*Corresponding author, Ph.D., Assistant Professor, E-mail: dykim2017@pusan.ac.kr
[a] Ph.D., E-mail: janghwan.kim1@gmail.com
[b] Ph.D., Assistant Professor, E-mail: shkee@dau.ac.kr
[c] Ph.D., Associate Professor, E-mail: geotech@hongik.ac.kr

ISSN: 1229-9367 (Print), 1598-6233 (Online)

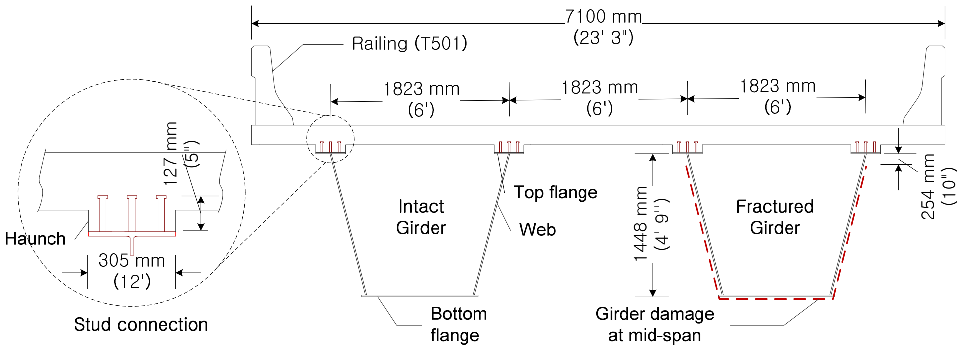

Fig. 1 Cross section of test bridge

redundancy based on a worst case loading scenario that could occur in a twin steel box-girder bridge. Using this method, the strength and displacement of the bridge can be directly evaluated simultaneously.

Compared to the studies on the redundancy evaluation methods, relatively limited research has been conducted to improve the redundancy of two girder bridges. Park *et al.* (2007) investigated the effect of a lateral bracing on the redundancy of two I-girder brides suffering one girder fracture. They found that the presence of the bracing could improve the redundancy of the bridge. Williamson *et al.* (2010) and Samaras *et al.* (2012) showed that the concrete deck of a twin steel box-girder bridge provides the main load redistribution path of the bridge suffering one girder fracture. If the redundancy of a two girder bridge could be improved by modulating such main bridge components providing a load redistribution path and the level of improvement could be quantitatively evaluated, bridge designers and bridge owners might control the level of the redundancy to the extent that the bridge could be considered as redundant. Therefore, there is a research need to investigate bridge components affecting the bridge redundancy and their contributions on it.

In this study, the various components of a twin steel box-girder bridge are investigated to evaluate their effects on the bridge redundancy. For this purpose, a detailed finite element model is constructed so that it could simulate critical aspects of responses that could occur in the ultimate behavior of the bridge required for the redundancy evaluation, such as large deflections, yielding of steel plates, concrete cracking or crushing, stud connection failure, and railing contacts over expansion joints. Based on the result of a full-scale bridge-fracture test conducted at the University of Texas at Austin (Williamson *et al*. 2010), the accuracy of the finite element (FE) model is proved and accordingly utilized for a parametric study to investigate the effects of various bridge components, such as railing, stud connection, and concrete deck, on the ultimate strength, stiffness, and the redundancy of the bridge. In the parametric study, three twin steel box-girder bridges with different span-to-girder depth ratios are utilized.

2. Damage level and loading scenario

Generally, a crack initiated on a tension member of a steel bridge gradually grows until its size becomes critical (Anderson 2017). Therefore, bridge members with such damage could be replaced or repaired through regular maintenance. However, it is not always possible to detect and fix such a crack before it becomes critical.

To evaluate the load-carrying capacity of the damaged bridge, the standard truck load (HS-20) specified in the AASHTO Bridge Design Specification (2014) is utilized. The HS-20 truck live load consists of three axle loads: a 36-kN (8-kip) front axle load, and 142-kN (32-kip) middle and rear axle loads. The distance between the front and the middle axles is fixed at 4.27 m (14 ft), whereas that between the middle and rear can vary from 4.27-9.14 m (14-30 ft). In this study, it is assumed that the rear axle is also 4.27 m (14 ft) away from the middle so as to maximize the loading effect on the bridge. The truck live load is applied on the bridge after the girder fracture damage is imposed on a section such that the maximum positive bending moment is induced by the truck load. To estimate the ultimate loading capacity, each axle load is increased proportionally beyond one truck loading. This loading configuration corresponds to placing one truck on top of other truck loads.

3. FE models for ultimate behavior evaluation

Numerical models for the ultimate response of the twin steel box-girder bridge are developed using ABAQUS/Standard 2017 which is a commercially available general purpose finite element analysis software package. The FE bridge models are constructed based on the test bridge as shown in Fig. 1. The test bridge had been in service for approximately nine years as a high-occupancy vehicle lane near the intersection of Interstate I-10 and Loop 610 in Houston, Texas. However, because this bridge was removed from service as a consequence of a highway expansion plan and the steel girders were transferred to the Ferguson Structural Engineering Laboratory at the University of Texas at Austin, where the deck and bridge rails were reconstructed. After its reconstruction, three separate tests were performed. The purpose of the first two was to investigate bridge performance in relation to the sudden loss of bridge components. The detailed information describing these tests is available in Neuman (2009) and Williamson *et al.* (2010). The third test—bridge fracture test—related to the objective of this research, which was to evaluate the ultimate behavior of a bridge sustaining a girder fracture.

The test bridge consisted of two trapezoidal box girders with a span of 36.58 m (120 ft). The girder depth was 1448 mm (4 ft 9 in), the bottom and top flange widths were 1194 mm (3 ft 11 in) and 305 mm (1 ft), respectively, as shown in Fig. 2. The web thickness was 12.7 mm (0.5 in), and the thicknesses of the bottom and top flanges were 19.1 mm (0.75 in) and 15.9 mm (0.63 in), respectively. The bridge was slightly curved with a radius of curvature of 416.05 m (1365 ft). The thickness of the concrete deck was 203.2 mm (8 in) with a 76.2-mm (3 in) haunch on each top flange. Three welded headed studs with a height of 127 mm (5 in) were utilized for each stud connection. The Texas DOT T501 safety rails were constructed on the bridge deck with expansion joints placed at every 9.14 m (30 ft) along the bridge span. Accordingly, an expansion joint was made at the midspan of the bridge.

The FE bridge models are constructed with various types of elements to provide a realistic representation of the box-girder bridge as shown in Fig. 2. The steel plates are modeled using eight-node shell elements (S8R) and the external brace members are modeled using two-node truss (T3D2) and beam elements, depending on the boundary conditions of the braces. Eight-node solid elements (C3D8R) are used for the concrete deck and railing of the bridge models. Reinforcement in the concrete is modeled with T3D2 elements embedded into the concrete elements. Simply supported boundary conditions are used in the FE bridge models. One end constrains the vertical, transverse, and longitudinal translations of girders and the other end constrains the vertical and transverse translations.

Traditional metal plasticity is adopted to represent the nonlinear behavior of the steel members, such as the reinforcement and steel box girders. For the concrete members, cast iron plasticity is used to incorporate the

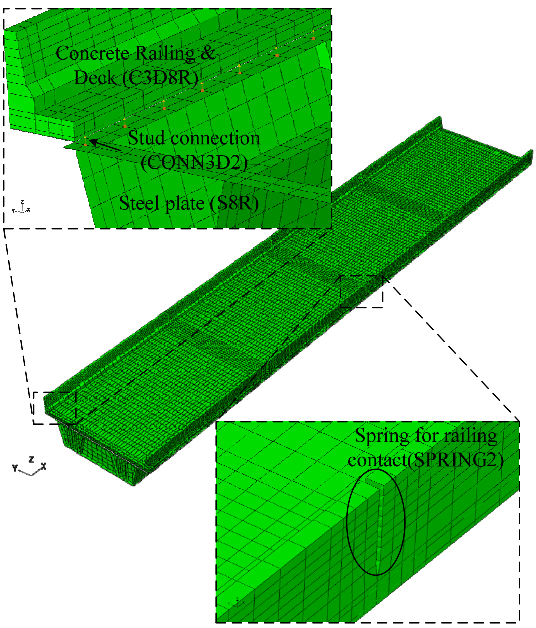

Fig. 2 Finite element bridge model

nonlinear behavior of concrete. In addition to material nonlinearities, railing contact and the failure of the stud connections are considered in the models using nonlinear spring (SPRING2) and connector (CONN3D2) elements, respectively. Details of the numerical simulations are described in the following sections.

3.1 Steel and concrete

The inelastic behavior of steel plates, brace members, and reinforcing steel are modeled using an elastic-perfectly plastic model with an isotropic hardening based on classical metal plasticity in both tension and compression (Dassault Systèmes 2017a). The yield strengths used for reinforcing steel and plates are 440 MPa (63.8 ksi) and 382 MPa (55.4 ksi), respectively, which were obtained from tension coupon tests conducted as a part of the research programs for the full-scale bridge fracture test. The assumed material density is 7849 kg/m^3 (490 lb/ft^3) for the reinforcement and steel plate.

There are two material models available in ABAQUS/ Standard 2017 for simulating the inelastic behavior of concrete: the concrete smeared cracking model and concrete damaged plasticity model. These models are capable of simulating tensile cracking and compressive crushing, including softening behavior beyond the failure surface of the material. However, full-scale bridge simulations with these material models, are not only computationally demanding but also difficult to converge into a solution. For this reason, in this study, the concrete deck and railing are modeled using a cast iron plasticity model which is less computationally demanding compared to the material models developed for concrete. The cast iron plasticity model was originally developed for gray cast iron, which has lower strength in tension than it does in compression similarly to concrete. To simulate the different strengths, a composite yield surface is utilized in the cast iron plasticity model where tension yielding is governed by the maiximum principal stress while compression yielding is governed by deviatoric stresses (Dassault Systèmes 2017b). Beyond the yield surface, a perfectly plastic behavior is assumed for the tension and compression, which is a primary difference between the concrete model and the cast iron. Despite such difference, it was shown that the cast iron plasticity model could be suitably applied to estimate the ultimate bending behavior of the concrete deck, by modulating the tensile strength to 4% of the compressive strength (Kim and Williamson 2015).

For the inelastic behavior of concrete, hardening rules in tension and compression should be defined with concrete compressive strength. In this study, the hardening curve for compression behavior is defined using Eq. (1), as suggested by Hognestad (Wight and Macgregor 2012) and the initial stiffness of the stress-strain curve in compression is used for the tension behavior.

$$f_c = f_c'' \left[\frac{2\varepsilon}{\varepsilon_o} - \left(\frac{\varepsilon}{\varepsilon_o} \right)^2 \right] \tag{1}$$

where f_c = concrete compressive stress at a given strain (ksi), $f_c'' = 0.85 f_c'$ (to account for the difference between cylinder and member strengths), f_c' = concrete compressive strength (ksi), ε = strain, and ε_o = strain at maximum stress.

Over time, the concrete compressive strength increases after curing and detailed strength data as function of time would be needed to account for the aging effect of the concrete components in the bridge model. However, in general, collecting concrete strength data for this purpose would not be practical. Instead, the equation (for concrete Type I under the moisture curing condition) recommended by ACI Committee 209 (Wight and Macgregor 2012) can be used to estimate the strength gain of concrete as a function of time, as indicated in Eq. (2). The measured average concrete compressive strength of the concrete deck for the full-scale test bridge was 33.4 MPa (4.84 ksi) obtained from the concrete cylinder tests at 28 days. Concrete density was determined to be 2323 kg/m^3 (145 lb/ft^3). The bridge fracture test was conducted approximately 32 months later (973 days) after the deck casting. Therefore, the estimated concrete strength for the full-scale fracture test is 39.1 MPa (5.67 ksi).

$$f_c'(t) = f_c'(28)\left[\frac{t}{4+0.85t}\right] \tag{2}$$

where f_c' (t) = concrete compressive strength at age t (ksi) and t = curing time (day).

3.2 Railing

Various types of bridge rails, differing in materials and shapes, are currently available in the bridge industry. The rails primarily function as safety barriers for vehicles on the bridge. Under normal conditions (i.e., without any damage on the bridge), the rails have negligible contribution to the overall loading capacity of the bridge because the metal railing has low bending strength and the concrete railing (T501) has gaps between rails for expansion joints. Therefore, the railing is not considered as a structural member and its contribution to the loading capacity is typically ignored. However, under a damaged condition, such as when one girder is fractured, the gap between the T501 railings could close when the bridge is largely deflected. In this case, the railing may act as an edge beam and bear some amount of the longitudinal bending moment of the bridge.

In this regard, a detailed contact analysis may be utilized to account for the engagement of the rail sections. However, for the contact analysis, a refined mesh density is required at the contact surfaces in order to obtain accurate results. Moreover, convergence problems could frequently arise when the analysis is related to nonlinear material properties (Dassault Systèmes 2017a). For the full-scale bridge modeling, significant computational resources are needed to create appropriate mesh refinements for such localized contact regions. Furthermore, material nonlinearities adopted in this study could lead to excessively long computational time and potentially prevent the convergence of the analysis because of the contact regions. For these reasons, a simplified modeling technique is utilized—spring elements are used to account for the engagement of the rail sections. Once the rails engage through the gap, it is possible that shear forces are transferred through friction. In this study, this effect is ignored in the FE simulations, and it is conservatively assumed that only normal forces are transferred through the railing contact. Note that no normal forces should develop in the spring elements before the rail gaps completely close. To simulate this behavior, spring elements designed to resist only compression forces are utilized. Displacement constraints are also applied on the load-displacement behavior of the spring elements such that they are effective when the compressive displacement exceeds 19.1 mm (3/4 in), which corresponds to the initial gap distance of the T501 railing for the test bridge. Once rail contact is initiated, the stiffness of the spring elements is determined using the elastic stiffness of the concrete to simulate the post contact behavior of the railing.

3.3 Stud connection

In the construction of the steel box-girder bridge, the stud connection is used to develop composite action by transferring mainly horizontal shear forces between the concrete deck and steel box girder. Typically, welded headed studs are utilized for the stud connections shown in Fig. 3 and cast into the concrete deck to provide mechanical shear transfer. In the FE bridge models, the stud connections have been typically modeled as rigid ties (Linzell and Nadakuditi 2011, Joo *et al*. 2015) or nodal constraints (Wu *et al*. 2015) without considering their potential failure mechanism. Nevertheless, this modeling approach provides good results when estimating the load-displacement behavior of a composite bridge without the girder fracture damage.

When the girder fracture damage is initiated, the deck deflects in a double curvature to transfer the applied load from the fractured girder to the intact girder, as shown in Fig. 4(a). In addition, high tensile forces are developed on the stud connections along the interior top flange of the fractured girder, which could lead to the failure of the connections. Once the stud connections fail, the bent shape of the deck changes into a single curvature, as shown in Fig. 4(b). Consequently, the bending strength and stiffness of the deck could be reduced (Samaras *et al*. 2012). For this reason, the detailed failure behavior of a stud connection under tensile forces combined with shear is needed to properly evaluate the ultimate behavior of the bridge. In this

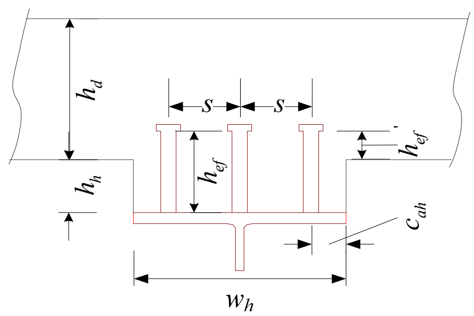

Fig. 3 Schematic of stud connection with haunch

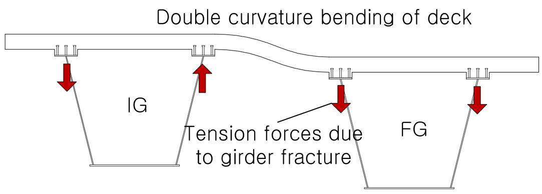

(a) Deflected shape before stud connection failure

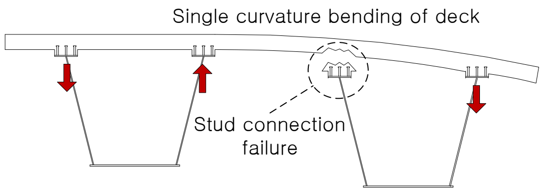

(b) Deflected shape after stud connection failure

Fig. 4 Deflection shape change by stud connection failure

study, connector (CONN3D2) elements are utilized in the FE models to represent the stud connections comprising of a group of studs, as shown in Figs. 2 and 3. The connector elements can be utilized in a three dimensional problem to connect two different parts with various kinematic constraints such as welding, a door hinge, and a constant velocity joint. The connector elements have relative displacements and rotations that are represented by six nodal degrees of freedom (Dassault Systèmes 2017a). The detailed element responses for the stud connections under shear and tension are described in the following sections.

3.3.1 Shear behavior of stud connection

Based on the shear test results of the stud connections comprising of welded headed studs, Topkaya (2002) proposed a nonlinear shear load-displacement relationship that could be utilized to define the constitutive relation of a connector element representing a stud connection in the FE model. The proposed relationship is as follows

$$Q = Q_d \frac{3\left(\dfrac{\Delta}{0.03}\right)}{1+2\left(\dfrac{\Delta}{0.03}\right)} \tag{3}$$

$$Q_d = 1.75 A_{sc}\left(f_c^{'} E_c\right)^{0.3} \tag{4}$$

where Q_d = design shear strength (kips), Δ = shear displacement of headed stud (in), A_{sc} = cross-sectional area of shear stud (in^2), $f_c^{'}$ = concrete compressive strength (ksi), and E_c = elastic modulus of concrete (ksi).

As indicated in Eq. (3), the shear load-displacement response of a stud connection could be determined by computing the design shear strength, Q_d. For example, the stud connection of the test bridge comprised of three 127-mm (5-in) long and 22.4-mm (7/8-in) diameter headed studs set in a row transversely as schematically shown in Fig. 3. The stud connection is modeled with a single connector element in the FE bridge models for simplicity, with a total cross-sectional area, A_{sc}, of 1164 mm^2 (1.8 in^2). Using Eq. (2), the compressive strength of concrete estimated for the test bridge is 39.2 MPa (5.69 ksi) and its relevant modulus of elasticity is 29.7 GPa (4300 ksi) based on the guidelines of ACI 318-14 (2014). Substituting these values into Eq. (4), the design shear strength, Q_d, for the constitutive relation of the connector element is determined as 291 kN (65.4 kips).

In addition to the shear load-displacement relationship, Topkaya (2002) also suggested an equation (Eq. (5)) to estimate the maximum shear strength for the stud connection. Although the maximum strength is not required to simulate the pure shear behavior of the connector element, it is necessary to compute the reduced design shear strength (Q_d) for shear load-displacement relationship because of shear-tension interaction, discussed later in this paper.

$$Q_u = 2.5 A_{sc}\left(f_c^{'} E_c\right)^{0.3} = 1.43 Q_d \tag{5}$$

3.3.2 Tensile behavior of stud connection

A stud connection comprising of welded headed studs shows the concrete breakout failure under tension. The tensile load-displacement relationship of the stud connection is linearly proportional until the load reaches its maximum strength. Beyond the maximum strength, the load quickly drops due to the brittle nature of the concrete (Sutton *et al.* 2014). To numerically model the tensile behavior of the stud connection, Kim and Williamson (2018) proposed a tensile load-displacement relationship, as shown in Fig. 5, based on the direct tension test results of stud connections performed by Sutton (2007) and Mouras (2008).

Sutton (2007) and Mouras (2008) conducted the direct tension test for stud connections and found that the tensile strength of a stud connection without a haunch configuration could be estimated using the concrete breakout strength equation of anchors in ACI 318-08, Appendix D.5.2 which corresponds to the provision in Section 17.4.2 of the recent ACI code (ACI 318 2014).

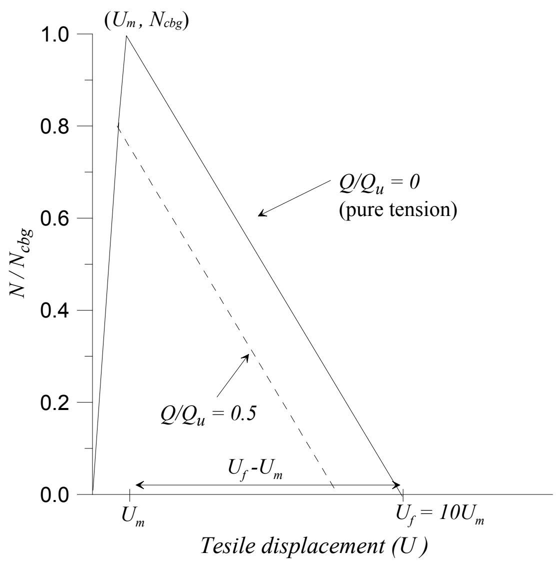

Fig. 5 Tensile load-displacement behavior

However, for a stud connection with a haunch, as shown in Fig. 3, the anchor strength equation specified in ACI 318 overestimates the tensile strength. To account for the haunch effect on the tensile strength, Kim and Williamson (2018) proposed a modified anchor strength equation with a haunch modification factor, $\psi_{h,N}$, as follows

$$N_{cbg} = \frac{A_{Nc}}{A_{Nco}} \psi_{h,N} \psi_{ec,N} \psi_{ed,N} \psi_{c,N} \psi_{cp,N} N_b \tag{6}$$

$$\psi_{ec,N} = \frac{1}{\left(1 + \dfrac{2e_N^{'}}{3h_{ef}}\right)} \tag{7}$$

$$\psi_{ed,N} = 0.7 + 0.3 \frac{c_{a,\min}}{1.5h_{ef}} \leq 1.0 \tag{8}$$

$$N_b = k_c \sqrt{f_c^{'}} h_{ef}^{1.5} \tag{9}$$

where A_{Nc} = projected concrete failure area of a single or group of anchors (in^2), A_{Nco} = projected concrete breakout surface area of a single anchor (= 9 $h_{ef}^{\,2}$, in^2), h_{ef} = effective embedment depth of an anchor (in), $\psi_{h,N}$ = haunch modification factor, $\psi_{ec,N}$ = modification factor for anchor groups loaded eccentrically, $\psi_{ed,N}$ = modification factor for edge effects, $\psi_{c,N}$ = cracked concrete modification factor (1.0 for cast-in anchors), $\psi_{cp,N}$ = modification factor for post-installed anchors (1.0 for cast-in-place anchors), N_b = concrete breakout strength of a single anchor (lb), k_c = 24 for cast-in anchors, and $f_c^{'}$ = concrete compressive strength (psi.).

$$\psi_{h,N} = 0.43 + 0.10\left(3.00 - 0.77\frac{h_{ef}^{'}}{h_{ef,\min}^{'}}\right)\left(\frac{c_{ah}}{c_{ah,\min}} - 1.0\right) \leq 1.0 \tag{10}$$

where $h_{ef}^{'}$ = modified effective embedment depth of an anchor into the concrete slab excluding the haunch height (= $h_{ef} - h_h$) (in), h_h = haunch height (in), $h_{ef,min}^{'}$ = minimum effective embedment depth (= 50.8 mm (2 in) – stud head thickness), c_{ah} = edge distance measured from the center of a stud to the haunch edge, and $c_{ah,min}$ = minimum edge distance (= minimum concrete cover specified in ACI 318-14+ half of the stud diameter).

To determine the tensile load-displacement relationship, the displacement U_m (where the maximum strength occurs) is required. Kim and Williamson (2018) conducted a data regression analysis to determine U_m as a function of the modified effective embedment depth of a stud utilizing the load-displacement data collected from the direct tension test for stud connections performed by Sutton (2007) and Mouras (2008). Based on the analysis, U_m was proposed, as follows

$$U_m = \frac{93h_{ef}^{'}}{h_d} \frac{\sqrt{f_c^{'}}\left(h_d + h_h\right)}{10^6} \tag{11}$$

where h_d = deck height (in).

In the full-scale test bridge, three 127-mm (5-in) long studs each with a 9.5-mm (3/8-in) head thickness were utilized and embedded into the concrete deck through the 76.2-mm (3-in) haunch (h_h) as schematically shown in Fig. 3. Therefore, the modified effective embedment depth ($h_{ef}^{'}$) is 41.3 mm (1-5/8 in) by subtracting the head thickness and haunch height from the embedment depth. The haunch edge distance (c_{ah}) was 50.8 mm (2 in) and deck height (h_d) was 203.2 mm (8 in). The modulus of elasticity of concrete is 29.7 GPa (4300 ksi) based on the guidelines in ACI 318-14 (2014). Therefore, from Eqs. (6) and (10), the estimated tensile strength is 69 kN (15.5 kips), and from Eq. (11), its corresponding displacement is 0.4 mm (0.02 in).

3.3.3 Shear-tension interaction

As previously discussed, high tensile forces with shear forces could be developed in the stud connection of a bridge sustaining one girder fracture. In this case, the shear and tensile strengths of the stud connection could be significantly reduced because of the interaction between the shear and tension forces. Therefore, it is necessary to incorporate strength reduction into the behavior of a connector element representing the stud connection to accurately estimate the ultimate strength of the bridge. The reduced strength can be determined according to the ACI guideline (ACI 318 2014) as follows

$$\left(\frac{N}{N_{cbg}}\right)^{5/3} + \left(\frac{Q}{Q_u}\right)^{5/3} = 1.0 \tag{12}$$

where N = applied tension force, Q = applied shear force, N_{cbg} = nominal concrete breakout strength of a group of anchors in tension from Eq. (6), and Q_u = shear strength computed from Eq. (5).

According to Eq. (12), the shear resistance is reduced to 80% of its maximum strength if the tensile demand corresponding to 50% of its tensile capacity exists on the stud connection and vice versa, as indicated in Figs. 5 and 6. Note that the load-displacement relationships under pure tension and pure shear in the figures show quite different post-yielding behaviors—brittle in tension and ductile in shear.

Once the tensile failure of a stud connection is initiated, any shear resistance mechanism is lost because of the brittle nature of the concrete breakout failure under tension forces. Therefore, because of the reduction effected by the shear-tension interaction, it is necessary to degrade the shear resistance under the combined loading condition below the maximum strength. In this study, a linear damage model suggested by Kim and Williamson (2018) is utilized to incorporate such strength degradation to diminish the shear resistance after the stud connection failure under combined forces, as shown in Fig. 6. In the linear damage model, to determine the degradation rate of the shear resistance, it is assumed that the residual shear displacement ($\Delta_f - \Delta_m$) is the same as the residual tensile displacement ($U_f - U_m$). This assumption is based on the inferred behavior of a stud connection failed under combined forces. At the initial stage of stud connection failure under tension forces,

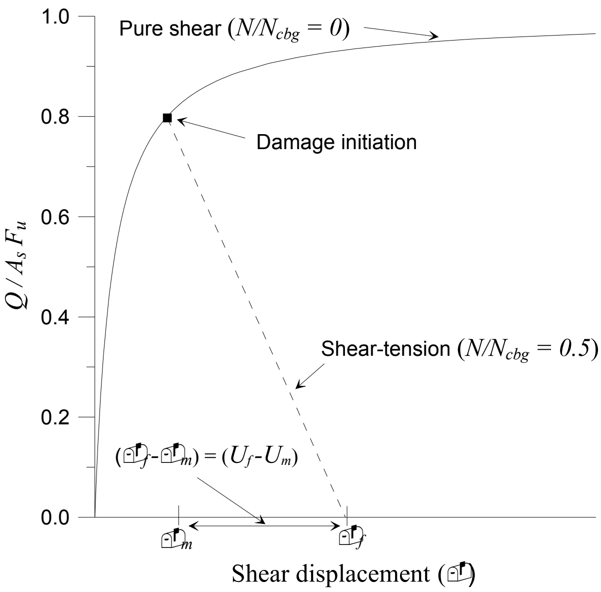

Fig. 6 Shear-displacement behavior

a portion of the shear loads may be transferred through cracks by interlocking between cracked concrete surfaces. Once the stud connection separates from the concrete deck due to concrete breakout failures, however, no shear-transferring mechanism remains. Therefore, it may be inferred that the stud connection starts to gradually lose its shear resistance after the initial stage of stud connection failure by tensile forces, and the shear resistance vanishes when the stud connection completely breaks out from the concrete deck

3.4 Simulation procedure

According to the damage level and loading scenario, the FE simulation procedure to evaluate the ultimate strength of a bridge sustaining one girder fracture can be categorized into three analysis groups: (1) bridge construction (steps 1–5), (2) girder fracture (step 6), and (3) load application (step 7), as described in the following:

(1) Deactivating the deck, railing, and rebar elements;
(2) Activating the dummy elements to trace the movement of the deactivated elements through girder displacement;
(3) Applying the gravity load to the girders and imposing the equivalent weight of the deactivated elements on the top flanges;
(4) Activating the deck, railing, and rebar elements with gravity load and removing the equivalent weight;
(5) Deactivating dummy elements;
(6) Applying girder fracture damage;
(7) Applying truck live load(s).

The bridge construction steps are intended to incorporate loading histories during the construction process, during which the bridge acts non-compositely. The elements deactivated in the first step, have no effect on mass and stiffness in ABAQUS. After deactivating these elements, pressure loads, equivalent to the self-weight of the concrete deck and railing, including the rebar, are evenly distributed on the top flanges of the girders. Before the concrete deck is cured, the deck and railing deform freely along with the girder deflection. To trace such a deformed position, dummy elements are used. The dummy elements share the same nodes with the original deck and railing elements, but they have no contribution on the bridge stiffness and weight. After this step, the concrete and railing elements are reactivated in the deformed position without strain changes, simulating the hardened concrete.

After the bridge construction analysis, a full-depth girder fracture (i.e., fracture on one of the girders) is applied at the location where the maximum positive bending moment caused by a moving vehicle occurs (e.g., at midspan for a simply supported bridge, such as the test bridge in this case). To mimic the girder fracture, duplicated nodes for shell elements along a fracture path are made and initially joined by connector elements with weld properties. The girder fracture can then be simulated by deactivating the connector elements. Once the bridge fracture is applied, then the live load is applied.

4. Full-scale bridge test and FE simulation

4.1 Full-scale bridge test

A full-scale bridge fracture test was performed to determine the ultimate load-carrying capacity of the twin steel box-girder bridge sustaining one girder fracture at the University of Texas at Austin (Williamson *et al*. 2010). In this research, the bridge fracture test is revisited to compare the primary failure modes and ultimate load-carrying capacity of a FE bridge model with test results.

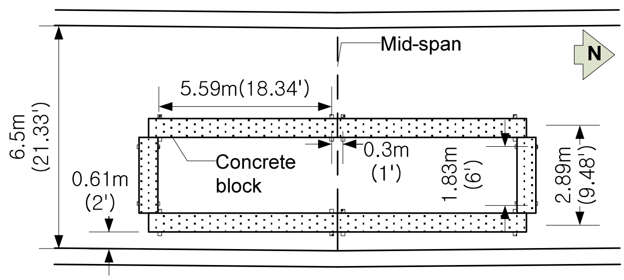

(a) Simulated load configuration

(b) Incremental loading process (Williamson *et al*. 2010)

Fig. 7 Loading configuration and process

To impose a damage corresponding to the girder fracture in the bridge fracture test, a torch was used to cut the web of one of the girders from the bottom flange to a point approximately 254 mm (10 in) below the top flange (i.e., 83% web removal) instead of a full-depth cut because of safety concerns. The damaged and undamaged girders were designated as fractured (FG) and intact (IG) girders, respectively, as indicated in Fig. 1.

To simulate the loading scenario (i.e., placing one truck on top of other truck loads), concrete blocks and load base were used, as shown in Fig. 7. As the concrete blocks were loaded, a crack initiated from the point where the torch cut was terminated and propagated towards the top flange. The concrete blocks were arranged in the form of a bin as shown in Fig. 7(a) so that the road base could be additionally loaded inside it. The total weight of the concrete blocks was 365 kN (82.1 kips). The concrete blocks were symmetrically placed about the bridge midspan but were transversely biased toward the fractured girder by setting 609.6 mm (2 ft) away from the east railing. This loading configuration was intended to mimic the worst loading condition that could be induced by the simulated truck loads.

The road base, consisting primarily of gravel and dirt, was placed using an air-operated lift bucket with a small backhoe, as shown in Fig. 7(b). The lift bucket was attached to the lifting hook of a crane. Once the bucket was filled, the weight of the road base was measured using a load cell attached to the end of the crane hook. After the crane lifted the bucket and weight was recorded, the lift bucket was positioned above the bridge and the road base was placed inside the concrete bin located on the bridge deck. The bridge finally collapsed when the total load imposed by the concrete blocks and road base reached 1614 kN (363 kips), corresponding to more than five times the HS-20 design truck load.

From visual inspections made during and after the bridge fracture test, the overall failure of the bridge was investigated. It was observed that the applied load was redistributed from the fractured girder to the intact girder through the concrete deck. The deck bent transversely in double curvature to transfer the load from the fractured girder to the intact girder. As the load increased, the conspicuous failure of the bridge components was initiated with the separation of the deck haunch (i.e., tensile failure of stud connections) along the interior top flange of the FG near the midspan, as shown in Fig. 8(a). This could have been caused by the tensile loading on the stud connections, increased by the transverse bending to transfer the applied load. Consequently, the tensile failure of the stud connections led to the change in the deflection shape of the concrete deck, as shown in Fig. 4.

As the loading increased, the failure of the stud connections was subsequently occurred along the outside of the fractured girder near the midspan. As the stud connection failure propagated along the bridge span, the bridge deck deflected largely near the midspan and the expansion joint at the top of the east railing was closed over most of its height as shown in Fig. 8(b). As the east railing started to crush, the stud connection failure along the interior top flange of the fractured girder continued to extend as did the stud connections along the outside of the fractured girder near the midspan. The bridge eventually collapsed when the stud connections failed along the entire length of the interior and exterior top flange of the fractured girder, as shown in Fig. 8(c).

(a) Stud connection failure (b) Railing crushing

(c) Bridge collapse

Fig. 8 Ultimate behavior of bridge (Williamson *et al*. 2010)

4.2 FE simulation for full-scale bridge test

To investigate the accuracy of the simulation model, the girder displacement and concrete strain of the railing collected from the full-scale bridge fracture test are compared with the simulation results. During the bridge fracture test, it was observed that the gap between the rails closed at the midspan. In the FE simulation of the bridge test, spring elements are used to account for the engagement of the rails at the midspan expansion joint, as previously mentioned.

Fig. 9(a) shows strain gauges installed on the top and side of the east railing above the fractured girder, and Fig. 9(b) compares the longitudinal strains obtained from the bridge test and FE simulation. As shown in Fig. 9(b), the railing starts to engage from the top and propagates to the bottom along the railing height. The simulated model captures the progressive contact of rails successfully, but the computed strains tend to deviate from the test result after railing contact initiates. This could be attributed to various factors, such as the spalling of the concrete cover, extensive crushing of the railing concrete, and non-uniform contact with the width of the railing. The large amount of the spalled concrete cover in the railing during the bridge fracture test, as shown in Fig. 8(b), suggests that the concrete strain gauge readings may not accurately represent the strain variation. Furthermore, the large deck deflection above the fractured girder could cause the rails to rotate about the longitudinal axis, resulting in the non-uniform

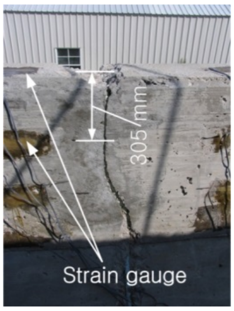

(a) Strain gauge setup (Williamson *et al*. 2010)

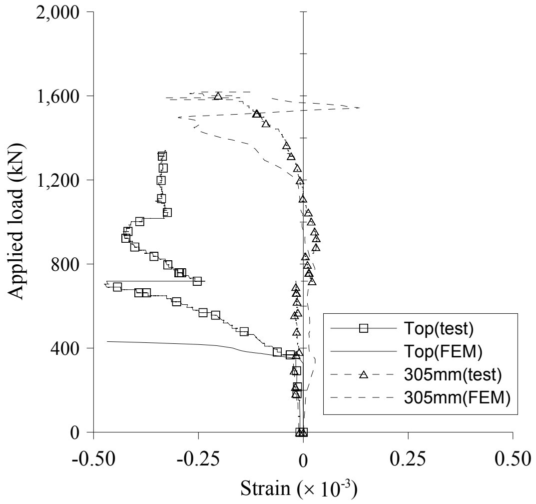

(b) Strain response through railing height

Fig. 9 Longitudinal strain response

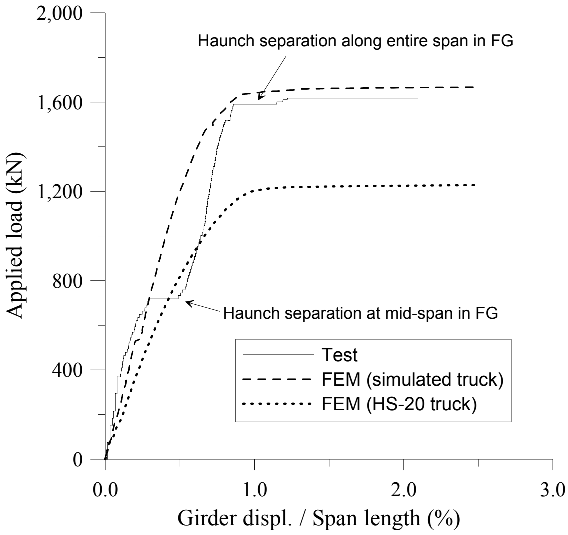

Fig. 10 Girder-displacement responses

contact with the width of the railing.

The displacement results of the fractured girder from the bridge fracture test and corresponding FE simulation are shown in Fig. 10. In this figure, the displacement is normalized with the bridge span. During the test, the girder displacement was measured at a location of 5.49 m (18 ft) away from the midspan. The measured and FE simulated data are indicated with solid and dashed lines, respectively.

During the test, as the applied load increased, the haunch along the interior top flange of the fractured girder was separated near the midspan and gradually extended along the span. Once the load reached approximately 689 kN (155 kips), there was a sudden deflection increase as indicated by a plateau in the displacement response. This sudden deflection was caused by the fracture of the stud connections from the outside of the fractured girder. The fracture of the stud connections was initiated near the midspan and suddenly extended approximately 6.1 m (20 ft) to the north and the south directions. When the applied load reached the maximum load of 1619 kN (364 kips), the entire haunch of the fractured girder was separated from the deck. Subsequently, the bridge collapsed.

As shown in Fig. 10, the overall load-displacement response of the FE simulation model agrees well with test data. The maximum load capacity estimated by the simulation is approximately 1664 kN (374 kips) which is only 3% higher than that of the bridge test result. However, different from that in the bridge test, the sudden fracture of the stud connections does not occur on the outside of the fractured girder in the FE simulation. Instead, it gradually occurs along the span of the fractured girder. Note that the test bridge had been damaged in the two preceding tests, but the rehabilitation of the bridge was not attempted before the bridge fracture test to evaluate its ultimate load-carrying capacity, which is the focus of this study. The FE model does not account for such damage from previous tests, which could be one of the reasons why the local failure behavior is different (i.e., sudden fracture of the stud connections on the outside of the fractured girder).

The assumed loading scenario to evaluate the load-carrying capacity of the bridge is to increase the axle loads of the HS-20 truck proportionally to the original axle loads of one truck. In the bridge fracture test, the concrete blocks and road base were used to simulate the loading scenario with the HS-20 truck loading configuration. The concrete blocks are modeled with concentrated loads and the load base is modeled with the pressure load in the FE simulation for the bridge fracture test. However, the simulated truck loading has a different loading configuration compared to the HS-20 truck, as shown in Fig. 7. To evaluate the difference between the loading configurations, the fractured girder displacement of the bridge model with the HS-20 truck loading is compared with that of the bridge model with the simulated loading.

The dotted line in Fig. 10 indicates the load-displacement response of the model utilizing the HS-20 truck loading configuration. Comparing the results of the HS-20 loading case with those of the simulated loading, the HS-20 truck loading configuration has a more severe loading effect than the simulated truck loading. This could be caused by the fact that the HS-20 loading modeled with concentrated loads has a longer lever arm for the transverse bending than the simulated loading because the road base of the simulated load is distributed over a wider region of the deck.

Table 1 Box girder and stud connection dimensions

Model	Box girder									Concrete deck	
	Span to girder depth ratio			Width (mm)			Thickness (mm)			Width (m)	Thk. (mm)
	Span (m)	Depth (m)	Span /Depth	Bottom	Between webs @ top	Top flange	Bot flange	Web	Top flange		
S24	51.8	2.2	23.7	1,130	2,134	457	38.1	19.1	38.1	8.1	203
	(170 ft)	(86 in.)		(44.5 in.)	(84 in.)	(18 in.)	(1.5 in)	(0.75 in.)	(1.5 in.)	(26.42 in.)	(8 in.)
S25	36.6	1.5	25.0	1,194	1,829	305	19.1	12.7	16.3	7.1	203
	(120 ft)	(57.7 in.)		(47 in.)	(72 in.)	(12 in.)	(0.75 in.)	(0.5 in.)	(0.64 in.)	(23.25 in.)	(8 in.)
S28	61.0	2.2	27.9	1,130	2,134	457	50.8	19.1	44.5	8.1	203
	(200 ft)	(86 in.)		(44.5 in.)	(84 in.)	(18 in.)	(2 in.)	(0.75 in.)	(1.75 in.)	(26.42 in.)	(8 in.)

5. Parameters affecting the ultimate behavior

The crushing of the railing and tensile failure of the stud connections in the full-scale bridge fracture test were identified as the prominent failure behaviors that need to be considered to investigate the ultimate loading capacity of the bridge. Therefore, changing the railing conditions and (or) stud connections could affect the ultimate behavior (i.e., the ultimate loading capacity and the stiffness) of the twin steel box-girder bridge. In addition to these factors, concrete compressive strength not only directly affects the transverse bending strength of the concrete deck but also influences the strength of the stud connections of the bridge. For these reasons, the railing, strength of the stud connection, and concrete strength are selected as variable parameters to investigate the ultimate behavior of the twin steel box-girder bridge in this study.

To investigate the effects of these parameters on the ultimate loading capacity and stiffness of the twin steel box-girder bridge, three simply supported bridges with varying span-to-girder depth ratios (i.e., 23.7 for the S24 model, 25 for S25, and 27.9 for S28) are simulated using FE models. Their load-displacement behaviors are evaluated in this section.

The dimensions of the bridges utilized for the simulation models are listed in Table 1. Among the three bridges listed in this table, two bridges (S24 and S28) are currently in service as exit ramps at Woodway near the intersection of I-10 and Loop 610 in Houston. S25 is the test bridge reconstructed at the Ferguson Structural Engineering Laboratory. In the FE simulations for the parametric study, the loading configuration of the HS-20 truck and concrete compressive strength of 27.6 MPa (4 ksi) are utilized except in the cases where the effect of the concrete strength is investigated.

5.1 Concrete railing

As demonstrated in the bridge fracture test, the T501 railing could act as an edge beam once the gap between the rails was closed by transferring normal forces through it. This implies that the railing could affect the ultimate behavior of the bridge. In this study, to investigate the contribution of the railing engagement on the ultimate loading capacity and stiffness of the twin steel box-girder bridge sustaining a fracture on one of the girders, the displacement responses of the FE models without the railing engagement effect (i.e., without the spring elements to account for the railing contact) are compared with those of the FE models with the railing engagement effect.

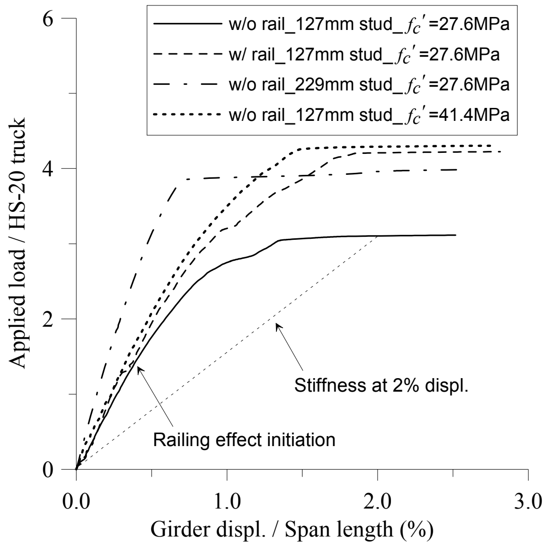

Fig. 11 Parameters affecting remained load-carrying capacity (S25 model)

The load-displacement behaviors of the S25 model (with a span-to-girder depth ratio of 25) are shown in Fig. 11. The solid and dashed lines compare the load-displacement behaviors between the bridge models with and without the railing engagement effect. The simulation result of the model with the railing engagement effect not only shows a 35% higher load-carrying capacity than the model without the railing engagement, but also a stiffer behavior beyond a displacement exceeding approximately 0.4% of the span. Note that Fig. 11 only shows the displacements caused by the live load after the girder fracture. According to the FE simulation, the calculated displacement by the girder fracture is 0.39 % of the bridge span. Therefore, the railing begins to be effective on the load-displacement response of the bridge when the displacement caused by the girder fracture and live load exceeds approximately 0.79 % of the bridge span.

To quantitatively evaluate the stiffness in the load-displacement behavior, a secant stiffness of 2% of the bridge span is computed, as illustrated in Fig. 11 for the S25 model without the railing effect. The 2% displacement is arbitrarily selected in this study, considering that all the investigated bridge models show perfectly plastic behaviors before the aforementioned displacement is reached. The stiffness of the S25 model without the railing is evaluated as 1.36 MN/m and is increased to 1.84 MN/m to account for the railing effect.

The ultimate load-carrying capacity and stiffness variations of the bridge models at different span-to-depth ratios are shown in Figs. 12 and 13. The ultimate capacity and stiffness tend to decrease as the span-to-girder depth ratio. This tendency could be attributed to the higher longitudinal bending moment induced by the applied truck live load in longer bridge spans. Within the range of the investigated bridge spans, the ultimate loading capacity and stiffness improved by the railing are indicated by the solid line with circle markers. The railing enhances the ultimate strength and stiffness from 6–35% and 7–36%, respectively.

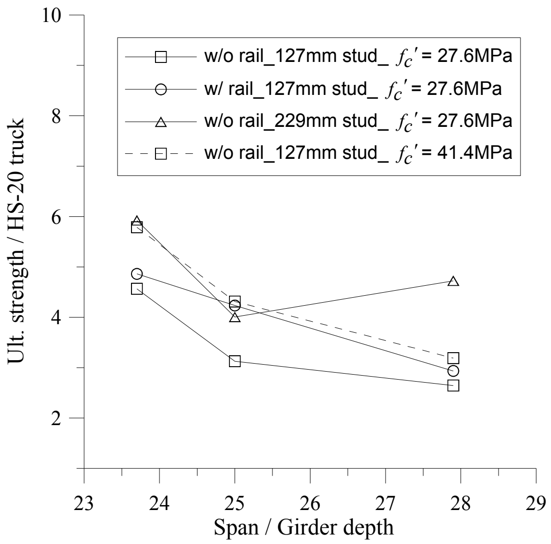

Fig. 12 Ultimate strength variation

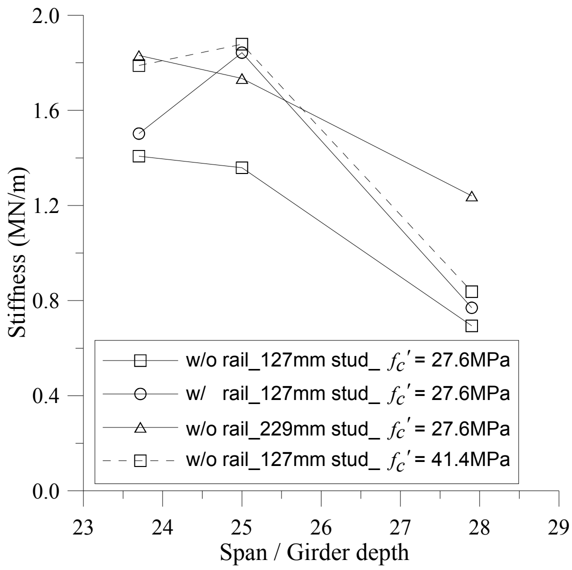

Fig. 13 Stiffness variation

5.2 Tensile strength of the stud connection

As mentioned previously, the applied load on the fractured girder could be redistributed to the intact girder through the transverse bending of the concrete deck, which causes high tensile forces on the stud connections of the fractured girder. Such high tensile forces could induce the stud connection failure on the interior flange of the fractured girder, resulting in the reduction of the bending strength and stiffness of the deck by changing the bending shape from a double curvature into single curvature (Samaras *et al*. 2012). Accordingly, the ultimate loading capacity and stiffness of the bridge could be affected by the tensile strength of the stud connection.

The tensile strength of a stud connection could be influenced by various factors such as the concrete strength, embedment depth of a stud(s), and presence of the deck haunch (Mouras 2008). Among these factors, the embedment depth of the stud could be modulated without any impact on the design of the other components of the bridge. For this reason, in this study, the tensile strength effect on the ultimate load-carrying capacity of the bridge is investigated by increasing the embedment depth of a stud. The stud connections of the investigated bridges comprise of three 127-mm long and 22.4-mm (7/8-in) diameter studs, as schematically shown in Fig. 3. The studs are embedded into the concrete deck through the 76.2-mm (3-in) haunch. The haunch edge distance (c_{ah}) is 76.2 mm for the S24 and S25 bridge models, and 50.8 mm (2-in) for the S25 model. To investigate the tensile strength effect on the ultimate loading capacity, the embedment depth of the stud is increased by increasing the stud length from 127 (h'_{ef} = 41.3 mm) to 229 mm (h'_{ef} = 143 mm). The dimensions and tensile strengths of the stud connections are summarized in Table 2. By increasing the stud length, it is estimated that the tensile strength increases from 69 (15.5)–136 kN (30.6 kips) for S24 and S28, and from 58 (13.1)–121 kN (27.2 kips) for S25 according to Eqs. (6) and (10).

The dotted-dashed and solid lines in Fig. 11 compare the load-displacement responses in S25 model. As shown in Fig. 11, the bridge model with 229-mm studs shows not only a higher ultimate loading capacity, but also a stiffer behavior compared to the model with 127-mm studs. Figs. 12 and 13 show that the increased tensile strength of the stud connection (indicated by the solid line with triangle markers) is effective to improve the ultimate loading capacity and stiffness of the other bridge models with different span-to-girder depth ratios. By increasing the stud length from 127 mm to 229 mm, the ultimate strength increases by 28 to 79% and the stiffness by 10 to 56%.

5.3 Concrete strength

Concrete strength could affect not only the strength of the deck, but also influence the shear and tensile strength of a stud connection. The concrete strength is related to the tensile strength of the stud connection because the concrete breakout strength of a single isolated stud, N_b, in Eq. (9) is proportional to the concrete strength (ACI 318 2014). As

Table 2 Stud connection dimensions

Item	S24 & S28	S25
h_d (mm)	203 (8.0 in)	203 (8.0 in)
h_h (mm)	76.2 (3.0 in)	76.2 (3.0 in)
$h_{ef}^{'}$ (mm) for 127 mm stud	41.3 (1.6 in)	41.3 (1.6 in)
$h_{ef}^{'}$ (mm) for 229 mm stud	143 (5.6 in)	143 (5.6 in)
c_{ah} (mm)	76.2 (3.0 in)	50.8 (2.0 in)
s (mm)	152 (6.0 in)	102 (6.0 in)
$\psi_{h,N}$ for 127 mm stud	0.44 (0.017 in)	0.44 (0.017 in)
$\psi_{h,N}$ for 228.6 mm stud	0.44 (0.017 in)	0.44 (0.017 in)
$\psi_{ec,N}$, $\psi_{ed,N}$, $\psi_{ep,N}$, and $\psi_{cp,N}$	1.00	1.00
$\psi_{c,N}$	1.25	1.25
N_b (kN) for 127 mm stud	125.4 (28.2 kips)	105 (23.6 kips)
N_b (kN) for 228.6 mm stud	247 (55.5 kips)	220 (49.5 kips)
N_{cbg} (kN) for 127 mm stud	69 (15.5 kips)	58 (13.0 kips)
N_{cbg} (kN) for 228.6 mm stud	136 (30.6 kips)	121 (27.2 kips)

indicated in Eq. (4), the shear strength of the stud connection increases as the concrete strength increases. Therefore, it is expected that the load-carrying capacity of the bridge could be improved with the increase in concrete strength. According to Russell (2003), the specified concrete strength used for bridge deck construction is typically in the range 27.6 (4)–55.2 MPa (8 ksi). To evaluate the concrete strength effect, the FE simulation model with a compressive strength of 27.6 MPa is compared to the model with a 41.4 MPa (6 ksi) strength.

The dotted line in Fig. 11 shows the load-displacement response of the model with the concrete compressive strength of 41.4 MPa. As expected, the ultimate loading capacity and stiffness are improved by increasing the concrete strength. In the investigated range of the span-to-girder depth ratio, the ultimate loading capacity is improved by 21 to 38% and the stiffness by 22 to 27%, as shown in Figs. 12 and 13.

6. Redundancy evaluation

Bridge redundancy can be described as the load capacity that a bridge continues to carry without undergoing excessive deformation after sustaining failure in one or more of its main structural members. This implies that the bridge should not only sustain specified damage and load level, but also its displacement within a tolerable limit. Therefore, a damage and loading scenario should be specified together with the tolerable displacement limit for the redundancy evaluation of the bridge. Kim and Williamson (2015) proposed a redundancy evaluation method that could be applied to twin steel box-girder bridges. As damage and loading conditions for the redundancy evaluation, they assumed that the sudden girder fracture occurs at a section where the HS-20 truck live load induces the maximum positive bending moment. As target safety levels under the damage and loading conditions, they utilized two limit states. First, the largest girder displacement is limited to 1% of the span. This displacement was proposed by Ghosn and Moses (1998) as a tolerable limit, which allows the bridge to maintain minimal functionality as bridge users evacuate after a sudden girder fracture occurs. Second, the strain on the concrete deck above the intact girder is limited to 0.003, corresponding to the initiation of a collapse mechanism at the onset of concrete crushing.

In this study, the redundancy of the bridge models varying in span-to-girder depth ratio from 23.7 (S24 model)–27.9 (S28 model), is evaluated utilizing the method proposed by Kim and Williamson (2015). As shown in the previous section, the ultimate load-carrying capacity and stiffness of the twin steel-box girder bridge, sustaining a fracture on one of its girders, could be improved by modulating the conditions of the railing, embedment depth of the stud, and concrete strength. For this reason, these are considered as variable conditions in investigating the redundancy.

The girder displacement results of the bridge models with varying conditions in the railing, embedment depth of the stud, and concrete strength are shown in Fig. 14 and the corresponding deck strains are listed in Table 3. According to the redundancy evaluation results, the 127-mm (5-in) stud models with and without the S28 railing fail to converge during the analysis because of the excessive displacement induced by the failure of the stud connections

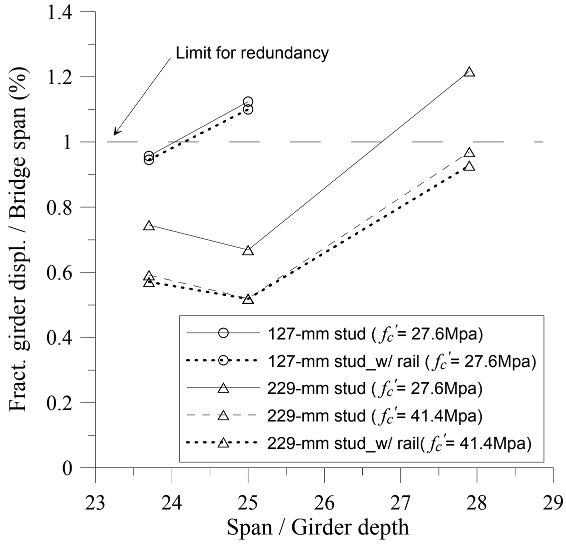

Fig. 14 Redundancy evaluation (girder displacement)

Table 3 Redundancy evaluation (deck strain)

Concrete strength	Model	Deck strain / 0.003 (%)		
		S24	S25	S28
Span length (m)		51.8	36.6	61.0
Span/depth		23.7	25.0	27.9
$f_c^{'}$ = 27.6 Mpa (4 ksi)	127-mm (5 in.) stud	98	83	-
	127-mm stud w/ rail	88	71	-
	229-mm (9 in.) stud	74	52	123
$f_c^{'}$ = 41.4 Mpa (6 ksi)	229-mm (9 in.) stud	50	49	86
	229-mm stud w/ rail	48	49	82

along the entire span of the fractured girder. For this reason, these cases are considered as non-redundant although they are not plotted in Fig. 14. As indicated by the solid line with circle markers in the figure, the 127-mm (5-in) stud model of S25 yields large girder displacements exceeding the tolerable limit (i.e., 1% of the bridge span) although the corresponding deck strains listed in Table 3 are within 0.003. A solid line with triangle markers shows the effect of the increased embedment depth. By increasing the 127-mm stud to 229 mm, the displacement of the S25 model is reduced within the limit qualifying it to be classified as redundant, whereas the displacement and strain of the S28 model still exceed the limits. By increasing the 27.6 MPa (4 ksi) concrete strength to 41.4 MPa (6 ksi), the displacement and deck strain of the S28 model decrease below the limits. These results imply that by modulating the embedment depth of the stud and (or) concrete strength, the displacement of the twin steel-box girder bridge could be improved to the extent that the bridge could be considered as redundant.

The dotted lines with circle and triangle markers show the effect of the railing on the redundancy of the 127- and 229-mm stud models, respectively. Different from the effect of increasing the embedment depth of the stud or concrete strength, modifying the railing does not significantly improve the displacements of the bridge models although it effectively improves their ultimate strength and stiffness. This discrepancy could be attributed to the fact that the railing only affects the load-displacement response when the bridge is largely deflected, as shown in the previous section. For instance, the railing begins improving the load-displacement response of the S25 model as the girder displacement caused by the damage and live load exceeds 0.79% of the span. In other words, the railing does not significantly affect the load-displacement response of the bridge within the 1% limit for the redundancy evaluation.

7. Conclusions

In this paper, a full-scale bridge fracture test and detailed FE modeling techniques are introduced to evaluate the ultimate load-carrying capacity of a twin steel-box girder bridge sustaining a fracture on one of its girders. The proposed FE model accounts for the nonlinear behaviors of the steel and concrete, railing contact, and stud connection failure under combined shear-tension loads that could occur before the applied load reaches the ultimate load capacity of the bridge. The ultimate capacity estimated by the FE model agrees well with the result of the full-scale bridge fracture test to within 3% difference. FE simulation conducted for various span-to-depth ratios demonstrate that the twin steel box-girder bridge could sustain a significant amount of load (i.e., approximately from 2.5 to 6 times the HS-20 truck load) even if it sustains a full-depth fracture on one of its girders, which is consistent with previous research (Williamson *et al*. 2010). This implies that this type of bridge could have a redundancy greater than that suggested by current design provisions to the extent that it might be classified out of the fracture-critical designation.

In the bridge fracture test, conspicuous local failures were observed in the T501 concrete railing and stud connections before the bridge collapsed. The railing exhibited a concrete crushing failure, acting as an edge beam after the gaps between the rail sections were closed because of the large deflection of the bridge. Moreover, the stud connections in the fractured girder were pulled out by high tensile forces induced by the transverse bending of the concrete deck. These imply that the railing and stud connections could have important functions in the load redistribution mechanism of the bridge with a girder fracture. For these reasons, the effects of the railing and tensile strength of the stud connection on the ultimate strength behavior and redundancy of the twin steel box-girder bridge are investigated in this study. Additionally, concrete compressive strength is also included as a variable parameter, considering that various concrete strengths are practically utilized in the bridge construction industry. The investigation considered three different bridge span-to-girder depth ratios, from 23.7–27.9.

The results of the parametric study using the proposed FE models show that the T501 railing, increased tensile strength of the stud connection, and the high strength concrete effectively increased not only the ultimate load-carrying capacity but also bridge stiffness. However, although the increased tensile strength and high concrete strength are effective in enhancing bridge redundancy, the railing does not significantly contribute to it when the displacement for the redundancy evaluation is limited to 1% of the bridge span. This is attributed to the fact that the railing only affects the load-displacement behavior when the bridge is largely deflected. In addition, there is a tendency for the ultimate loading capacity and stiffness to decrease as the span-to-girder depth ratio increases. In other words, the longer bridge span is, the higher is the tendency of the bridge to be non-redundant when the displacement is limited to 1% for the redundancy evaluation. Nevertheless, by modulating the tensile strength of the stud connection and (or) concrete compressive strength, the redundancy of the bridge could be enhanced for it to be excluded from its fracture-critical designation. This study suggests that although the twin steel box-girder bridge could be fracture critical (i.e., non-redundant) depending on its span-to-girder depth ratio, it could also be adjusted to become redundant by modulating the tensile strength of the stud connection and (or) concrete strength.

Acknowledgments

This research was supported and funded by Basic Science Research Program through the National Research Foundation of Korea (NRF) funded by the Ministry of Education (2016R1A6A1A03012812).

References

AASHTO (2014), LRFD Bridge Design Specifications; AASHTO, Washington, D.C., USA.

ACI 318 (2014), Building code requirements for structural concrete and commentary; ACI, Farmington Hills, MI, USA.

Anderson, T.L. (2017), *Fracture Mechanics*, (4th Ed.), CRC Press, Boca Raton, FL, USA.

Connor, R.J., Dexter, R. and Mahmoud, H. (2005), "Inspection and management of bridges with fracture-critical details", NCHRP Synthesis 354, Transportation Research Board, Washington, D.C., USA.

Connor, R.J., Kaufmann, E.J., Fisher, J.W. and Wright, W.J. (2007), "Prevention and mitigation strategies to address recent brittle fractures in steel bridges", *J. Bridge Eng*., **12**(2), 164-173.

Dassault Systèmes (2017a), ABAQUS Analysis User's Manual; ABAQUS, Inc., Rising Sun Mills, RI, USA.

Dassault Systèmes (2017b), ABAQUS Theory Manual; ABAQUS, Inc., Rising Sun Mills, RI, USA.

Ghosn, M. and Moses, F. (1998), "Redundancy in Highway Bridge Superstructures", NCHRP Report 406; National Academy Press, Washington, D.C., USA.

Hesse, A.A., Atadero, R.A. and Mahmoud, H.N. (2014), "Approach-span failure of the Hoan Bridge as a case study for engineering students and practicing engineers", *J. Perform. Constr. Fac*., **28**(2), 341-348.
DOI: 10.1061/(ASCE)CF.1943-5509.0000403

Joo, H.S., Moon, J., Sung, I. and Lee, H. (2015), "Moment redistribution of continuous composite I-girder with high strength steel", *Steel Compos. Struct., Int. J.*, **18**(4), 873-887.

Kim, J. (2010), "Finite Element Modeling of Twin Steel Box-Girder Bridges for Redundancy Evaluation", Ph.D. Dissertation; The University of Texas at Austin, Austin, TX, USA.

Kim, J. and Williamson, E.B. (2015), "Finite-element modeling of twin steel box-girder bridges for redundancy evaluation", *J. Bridge Eng*., **20**(10), 04014106.
DOI: 10.1061/(ASCE)BE.1943-5592.0000706

Kim, J. and Williamson, E.B. (2018), "Ultimate behavior of stud connections within haunches", *J. Bridge Eng*., **24**(1), 04018106.
DOI: 10.1061/(ASCE)BE.1943-5592.0001333

Linzell, D.G. and Nadakuditi, V.P. (2011), "Parameters influencing seismic response of horizontally curved, steel, I-girder bridges", *Steel Compos. Struct., Int. J.*, **11**(1), 21-38.

Mouras, J.M. (2008), "Evaluating the redundancy of steel bridges: improving the strength and behavior of shear stud connections under tensile loading", M.S. Thesis; The University of Texas at Austin, Austin, TX, USA.

Neuman, B.J. (2009), "Evaluating the redundancy of steel bridges: full-scale destructive testing of a fracture critical twin box-girder steel bridge", M.S. Thesis; The University of Texas at Austin, Austin, TX, USA.

Park, Y., Joe, W., Hwang, M. and Yoon, T. (2007), "After-fracture redundancy in simple span two-girder steel bridge", *Struct. Eng. Mech., Int. J.*, **27**(6), 651-670.

Pham, H., Doust, S., Yakel, A. and Azizinamini, A. (2014), "Comprehensive Evaluation of Fracture Critical Bridges", Rep. SPR-P1(09) P321; Florida International University, Miami, FL, USA.

Russell, H.G., Miller, R.A., Ozyildirim, H.C. and Tadros, M.K. (2003), "Compilation and evaluation of results from high performance concrete bridge projects—final report", *Proceedings of 3rd International Symposium on High Performance Concrete and PCI National Bridge Conference*, Orlando, USA, October.

Samaras, V.A., Sutton, J.P., Williamson, E.B. and Frank, K.H. (2012), "Simplified method for evaluating the redundancy of twin steel box-girder bridges", *J. Bridge Eng*., **17**(3), 470-480.

Sutton, J.P. (2007), "Evaluating the redundancy of steel bridges: effect of a bridge haunch on the strength and behavior of shear studs under tensile loading", M.S. Thesis; The University of Texas at Austin, Austin, TX, USA.

Sutton, J.P., Mouras, J.M., Samaras, V.A., Williamson, E.B. and Frank, K.H. (2014), "Strength and ductility of shear studs under tensile loading", *J. Bridge Eng*., **19**(2), 245-253.

Topkaya, C. (2002), "Behavior of Curved Steel Trapezoidal Box Girders during Construction", Ph.D. Dissertation; The University of Texas at Austin, Austin, TX, USA.

Wight, J.K. and Macgregor, J.G. (2012), *Reinforced Concrete Mechanics & Design*, (6th Edition), Pearson, New York, NY, USA.

Williamson, E.B., Frank, K.H., Samaras, V.A., Kim, J., Neuman, B.J., Sutton, J.P., Mouras, J.M., Hovell, C.G. and Barnard, T. (2010), "Modeling the Response of Fracture Critical Steel Box-Girder Bridges", Rep. FHWA/TX-08/0-5498-2; U.S. Dept. of Commerce, Alexandria, VA, USA.

Wu, J., Frangopol, D.M. and Soliman, M. (2015), "Simulating the construction process of steel-concrete composite bridges", *Steel Compos. Struct., Int. J.*, **18**(5), 1239-1258.

CC